Average patterns and coherent phenomena in wide aperture lasers

G. D'Alessandro

Department of Mathematics, University of Southampton, Southampton, SO17 1BJ, England, United Kingdom

F. Papoff

Department of Physics and Applied Physics, University of Strathclyde, 107 Rottenrow, Glasgow G4 0NG, Scotland, United Kingdom

E. Louvergneaux and P. Glorieux

Laboratoire PhLAM, Université de Lille 1, 59655 Villeneuve d'Ascq cedex, France

Using a realistic model of wide aperture, weakly astigmatic lasers we develop a framework to analyze experimental average intensity patterns. We use the model to explain the appearance of patterns in terms of the modes of the cavity and to show that the breaking of the symmetry of the average intensity patterns is caused by overlaps in the frequency spectra of nonvanishing of modes with different parity. This result can be used even in systems with very fast dynamics to detect experimentally overlaps of frequency spectra of modes.

I. INTRODUCTION

Time averaged patterns are the most common way to characterise the spatial complexity of large aperture lasers operating in the multimode regime. These patterns are generic: observation on CO_2 lasers [1–3] and solid state microchip lasers [4] are strikingly similar despite the differences between the physical processes involved in the emission of light. Moreover, average patterns are "robust," in the sense that they are insensitive to the details of the dynamics. For example, they may have an ordered appearance even though the underlying dynamics is not regular. This is true for optical patterns [1–5] as well as for patterns observed in hydrodynamics experiments involving thermal convection [6], surface waves [7–9], or electroconvection [10] where the slow dynamics allows for easy visualization of the instantaneous wave patterns. Arguably the appearance of average patterns in hydrodynamics is influenced by the boundaries [10,11] and their symmetries. An analogous situation holds for lasers: average intensity patterns in cavities with low Fresnel number clearly reflect the structure of the empty cavity modes [1,3,4]. Patterns in large Fresnel number cavities, where the effect of the curved mirrors is weakened, have an apparently rectangular symmetry. However, the shape and symmetry of average patterns vary as the control parameters are changed. A careful analysis shows that these variations depend upon the energy and the average products of amplitudes of different modes, which we call average amplitude products in the following. Therefore, the study of average patterns provides useful information especially in systems, such as lasers, where the instantaneous intensity patterns are not generally measurable due to the fast time scales of the dynamics. In fact, instantaneous measurement of the intensity pattern of a wide aperture laser are possible [12,13] as snapshots taken at different times in different pulses. It is not yet possible to measure the instantaneous intensity pattern of a laser over a continuous stretch of time. Even more difficult is to gather the phase information needed to reconstruct the field from the intensity.

The aim of this paper is to clarify some of the issues relating to average intensity patterns in medium Fresnel number lasers, i.e. patterns that are generated by the coupled dynamics of five to twenty modes away from the laser switching on threshold (first threshold), a situation very easily obtained in experiments. The number of modes is too high for the analytical study of the normal forms of the laser [14] and it is too low for order parameter equations [15,16]. Furthermore, both these techniques can be applied safely only close to first threshold, a condition that does not apply to the experiments we are considering.

The experimental observations in a CO_2 laser, detailed in Ref. [1,3] and summarized here in Sec. II, show that as the detuning of the cavity with respect to the atomic line is varied, different average intensity patterns appear. Some of them can be reproduced by incoherent superposition of Gauss-Hermite modes [3] that belong to the same family, minimize the spatial hole burning and maximize the energy extraction from the pump. Most patterns, however, do not fit this scheme.

The same type of patterns of Refs. [1,3] were observed in a microchip laser in Ref. [4]. The results of both experiments lead to many open questions which we address in this paper. First of all, we investigate the effect of the hard apertures present in the experiment of Ref. [3] on the modes of the cavity and on average patterns. Then we consider what is the most efficient modal description of the average intensity patterns far away from threshold. Finally, we investigate the role of symmetry: as a general rule, average patterns are more symmetric than the spatiotemporal dynamics of the laser from which they originate. We show how average symmetry can be used to analyze average amplitude products.

We address the above questions by calculating the modes of a cavity with intracavity aperture and deriving a model of the experimental laser from first principles. We integrate it numerically, both using the full integral-differential equations and by using a decomposition of the field into empty cavity modes. Both these techniques produce average patterns that are in good agreement with experimental patterns

of a CO_2 laser. We then use the model to study in detail aspects of laser patterns that extend the results of the experiments of Refs. [1,3,4]. In the following paper [17] we analyze the spatiotemporal complexity of the average patterns and its behaviour as the intensity of the pump is increased.

The rest of the paper is organized as follows. In Sec. II we describe the experimental setup and summarise the experimental observations on average patterns in CO_2 lasers operated in the domain of intermediate complexity. We derive a model of the experimental laser and analyze its modes in Sec. III. Section IV contains a theoretical analysis of the symmetry of the average patterns that is used in Sec. V to analyze numerical average intensity patterns. In the conclusions of this first paper we discuss briefly measures of symmetry and their application to experimental and numerical patterns.

II. EXPERIMENTAL RESULTS

The experimental patterns relevant to the analysis in this paper have been observed [1,3] at intermediate Fresnel numbers ($1 < N_f < 6$) in a wide aperture, astigmatic CO_2 laser whose modes are approximately Gauss-Hermite modes [18]. The astigmatism, caused by Brewster windows, lifts the frequency degeneracy of the modes that belong to the same family by introducing an intermode frequency splitting $\Delta_a \simeq 200$ kHz. Moreover, an iris present in the cavity to control its aperture, modifies deeply the structure of the wider cavity modes so that they can no longer be considered as Gauss-Hermite modes (see Sec. III). The experimental control parameters are as follows.

(1) The Fresnel number $N_f = S/(\pi S_0)$, i.e., the ratio of the cavity aperture area S to the fundamental mode maximal area S_0. N_f is an evaluator of the maximum transverse family index that can oscillate within the laser with small diffraction losses.

(2) The transverse interfamily frequency spacing $\Delta \nu_T$ [18] that rules the strength of the interaction between transverse modes belonging to different families. Since this quantity ($\Delta \nu_T = 0-5$ MHz) is always much smaller than the homogeneous linewidth ($\Delta \nu_H = 500-700$ MHz), multitransverse mode operation is possible in our large area laser. However, by keeping the pump sufficiently low it is also possible to excite a single family of modes.

(3) The position of the different family modes with respect to the center of the gain line.
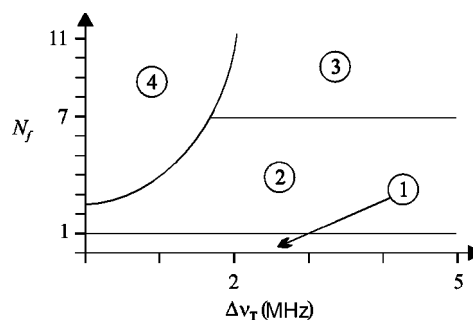
FIG. 1. Schematic representation of the different regions of pattern formation at a fixed pump value as a function of the Fresnel number N_f and the intertransverse mode spacing $\Delta_{\nu T}$ obtained from the experimental results of Refs. [1,3]. See text for the characteristic features of each region.

The general phenomenology of the experimentally observed patterns is depicted in Fig. 1. At low Fresnel numbers, typically $N_f \simeq 1$, only the first two or three transverse families may oscillate. This domain has been extensively investigated (see, e.g., Refs. [19–21]). In regions 2 (3), complicated patterns are observed with an intricate radio-frequency spectrum of the intensity at any point in the transverse profile. However for some particular settings of the cavity, this spectrum simplifies into regularly spaced clusters (Fig. 4 of Ref. [1]) associated to circular (region 2) and rectangular (region 3) pattern lattices that we call regular patterns (see Fig. 2 of Ref. [1] for images of regular patterns and Refs. [1,3] for an extensive discussion of their properties). This does not occur in region 4 where radio-frequency spectra and transverse patterns are always complicated. Regular patterns are classified as 0-0, 0-1, 1-0, or 1-1 according to whether they have minima (0) or maxima (1) of the intensity on the two symmetry axes.

In this paper we focus our attention to patterns in region 2 of Fig. 1. Here regular patterns are common, but not generic. In Fig. 2, for example, we show how there is an entire spectrum of "irregular" patterns that connects regular patterns as the cavity detuning is changed.

The relatively frequent appearance of regular patterns in the experiment is a minimal test to validate a model of the experiment: simulations should be able to produce regular patterns for appropriate values of the parameters. In particular, in all regular patterns the near field and the far field remain the same, indicating that the patterns are composed of modes of the same transverse family. Indeed, the Gouy phase
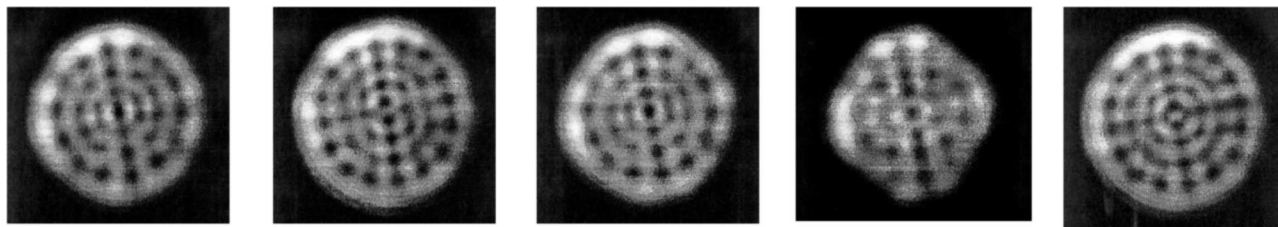
FIG. 2. Experimental near field images of the average intensity patterns showing a transition between a 1-0 regular pattern (far left) to a 0-0 pattern (far right) through some irregular patterns as the cavity detuning is changed. The images are stationary patterns measured after each change of the detuning.

shift [22], which is different for each transverse family, induces a far field different from the near field as soon as the modes composing the pattern belong to at least two families with indexes m of different parity.

Moreover, the number of rings varies from 1 to 6 following a linear dependence law versus N_f [1] as predicted by Siegman [23]. In other words, the patterns obey the same scaling laws versus the mode order m as the Gauss-Hermite or Gauss-Laguerre modes of the empty cavity. This is an indication that the observed ring patterns should be well described by the empty cavity modes, the Gauss-Hermite modes. In fact, in Ref. [3] it was shown that the regular patterns can be reconstructed using the *intensities* of Gauss-Hermite modes. This result is doubly significant: firstly it indicates that the cavity modes are, at least in the case of the observed patterns, very similar to Gauss-Hermite modes. Secondly, the intensity of the field is the modulus square of the sum of the modal amplitudes. This is equal to the sum of the squares of the moduli of the modal amplitudes only if the average amplitude products are negligible. We comment on these two points in Secs. III and V, respectively.

III. THE MODEL

The observation of the same type of average patterns in microchip and CO_2 lasers suggests that they are determined mainly by the geometry of the cavity rather than the nature of the active medium. Therefore, in order to perform our analysis, we improve the standard mean field limit Maxwell-Bloch laser model [24] by describing in more detail the geometry of the cavity and the propagation of the field inside it.

For simplicity we assume that the laser under study is a ring cavity gas laser with approximate cylindrical symmetry (see the end of Appendix A for a brief discussion of Fabry-Pérot cavities). The final equations are (A13)–(A15) reproduced here for convenience:

$$\frac{\partial F}{\partial t} = \mathcal{L}F + P, \tag{1}$$

$$\frac{\partial P}{\partial t} = -P + \chi F + FN, \tag{2}$$

$$\frac{\partial N}{\partial t} = -\gamma \left[N + \frac{1}{2}(F\bar{P} + \bar{F}P) \right], \tag{3}$$

where $F(x,y,t)$ and $P(x,y,t)$ are the slowly varying amplitudes of the electric field and polarization respectively, $N(x,y,t)$ is the population inversion, γ is the decay rate of the population inversion and χ is the pump parameter. All spatial and temporal variables are nondimensional and (x,y) are the coordinates in the transverse plane. The propagation across the cavity is taken into account by the operator $\mathcal{L} \equiv -c[Id - \mathcal{P}\Theta_A]$, where c is the speed of light, $\mathcal{P}$ is the propagation operator, defined in Eq. (A4), and $\Theta_A(x,y)$ represents the aperture, Eq. (A3). These equations constitute the model that we analyze in this paper.

The modes of the cavity without aperture are Gauss-Hermite modes [18]. The presence of the aperture couples

these modes together so that the new modes of the cavity are the eigenvectors of the propagation operator $\mathcal{P}$ defined in Eq. (A5). Note that as long as the aperture is circular and centred on the cavity axis, it does not change the rectangular symmetry of the cavity. As a consequence, the eigenvectors of $\mathcal{P}$ have definite parity and are either even or odd under reflections σ_x and σ_y about the symmetry axes x and y and under inversion $\sigma_x \sigma_y$ with respect to the origin. To find the modes of the cavity we have projected $\mathcal{P}$ on a large set of Gauss-Hermite modes (all the modes with $0 \leq m \leq 30$) obtaining an approximate matrix representation of this operator. The results of the modal analysis are summarized in Fig. 3 and confirm the intuitive hypothesis at the basis of the analysis of the experimental patterns used in Ref. [3]: if the modes are significantly narrower than the diameter of the aperture they are nearly Gauss-Hermite modes in the sense that a single Gauss-Hermite mode dominates the decomposition of the cavity modes on the Gauss-Hermite basis. This is confirmed by the graphs inserted in Fig. 3 that represent the modulus of the coefficients of the expansion of selected cavity modes on the basis of the Gauss-Hermite modes. Narrow cavity modes form families with almost degenerate frequencies. Similarly to the pure Gauss-Hermite modes, we can assign a label $m \in \mathbb{N}$ to each family of $m+1$ cavity modes. Modes of families with m even are even under inversion $\sigma_x \sigma_y$. These modes can be further divided into two subsets that are either even or odd under σ_x and σ_y. Similarly, modes of families with m odd are odd under inversion. These modes form two subsets, one of modes even under σ_x and odd under σ_y, the other of modes odd under σ_x and even under σ_y. However, as the diameter of the modes increases the cavity modes become more and more different from the Gauss-Hermite modes to the point that they are no longer grouped in nearly degenerate families, but span the entire free spectral range in a nearly continuous manner. Of course, as the modes become wider their losses increase so that it becomes harder and harder to excite them. As the diameter of the modes is related to the index m, the aperture determines the maximum index m_M such that for all $m \leq m_M$ the modes are almost Gauss-Hermite modes.

IV. SYMMETRY AND AVERAGE AMPLITUDE PRODUCTS

Before studying numerically the average patterns in the model, we analyze the symmetry of average intensity patterns in an astigmatic laser and how this can be used to detect the presence of nonvanishing average amplitude products. We consider here patterns whose Fourier spectra have a discrete number of peaks bounded away from zero, such as the spectra in Fig. 4 of Ref. [1] and Fig. 5 here. Except for this requirement, the analysis presented here is general and does not depend upon the presence of an aperture. For laser without apertures, or lasers whose cavity modes are only weakly perturbed by the aperture, the symmetry of the average intensity patterns reveals also if the laser near and far fields are self-similar.

Many of the average intensity patterns observed in astigmatic wide aperture CO_2 [1,3] lasers and in microchip [4] lasers presenting regularities (e.g., σ_x and σ_y symmetry) fall
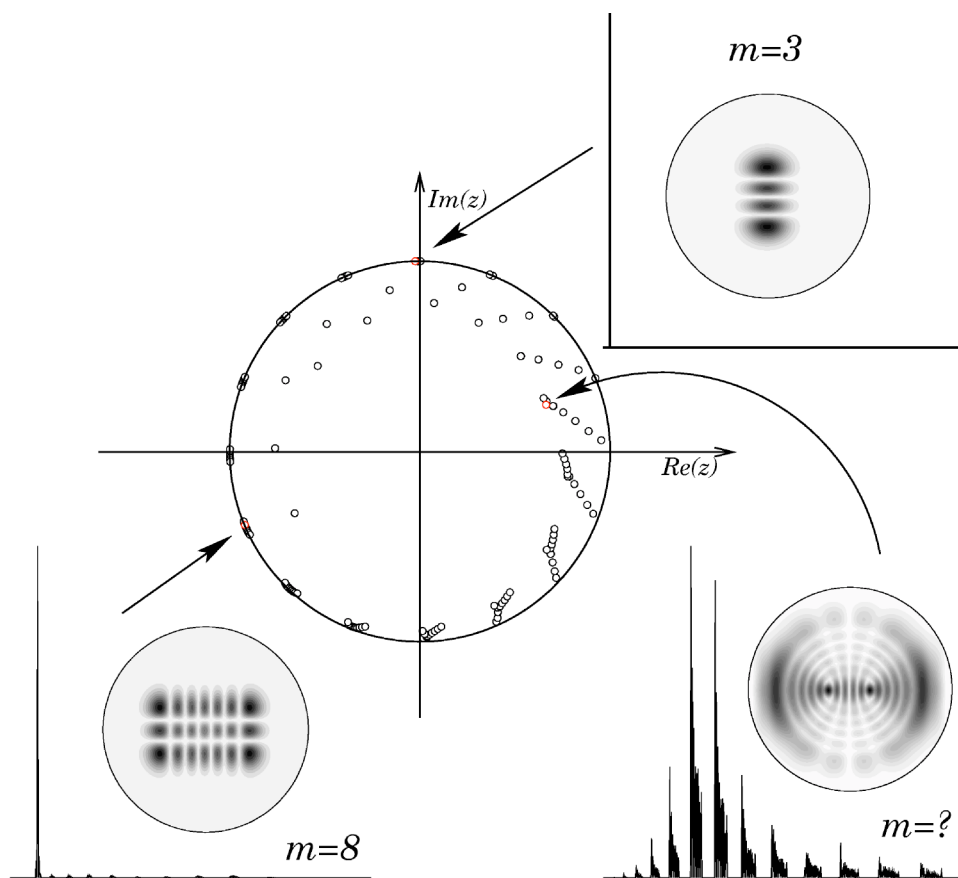
FIG. 3. Point spectrum of the propagation operator (A4) in the complex plane. The circle has unit radius: the closer the eigenvalues are to it, the smaller the loss of their corresponding cavity mode. Only the eigenvalues with modulus larger than 0.7 have been plotted. Modes that have beam waist smaller than the aperture radius are essentially Gauss-Hermite modes and have low losses. They are also grouped in nearly degenerate families, as are the Gauss-Hermite modes. The losses increase with the beam waist and large cavity modes are not well identified with a single Gauss-Hermite modes. The three inserts contain a grey scale image of the intensity of the selected cavity mode and a graph of the modulus of the coefficients of its expansion on the basis of the Gauss-Hermite modes of the aperture-less empty cavity. The circles in the intensity images have radius equal to five beam waists.

into one of the regular patterns discussed previously. Moreover, the intensity patterns observed in the CO_2 laser experiment can be well reproduced by superpositions of the intensity of subsets of the Gauss-Hermite modes of the empty cavity, namely those modes that are nearly degenerate in frequency and that are closest to resonance. This last observation implies that the average over long times of the products of amplitudes of pairs of modes is zero. This can be shown to be valid for generic stable cavities by writing the electric field of the laser $F(\boldsymbol{x},t)$, with $\boldsymbol{x}=(x,y)$, as a linear combination of the modes $A_k(\boldsymbol{x})$ of the empty cavity:

$$F(\boldsymbol{x},t) = \sum_{k=1}^{M} \bar{f}_k(t) A_k(\boldsymbol{x}), \qquad (4)$$

where M is the number of active modes, the overbar indicates complex conjugate, and $\bar{f}_k(t)$ is the time-dependent amplitude of the mode k. We use $\bar{f}_k(t)$ in this equation instead of $f_k(t)$, the standard notation of laser physics, in order to make the notation simpler in the accompanying paper [17]. The average intensity of the laser field is given by

$$\langle |F|^2 \rangle_{\mathcal{T}} = \sum_{j,k=1}^{M} \langle f_j \bar{f}_k \rangle_{\mathcal{T}} \bar{A}_j(\boldsymbol{x}) A_k(\boldsymbol{x}), \qquad (5)$$

where $\langle \cdots \rangle_{\mathcal{T}}$ indicates the average in time over an interval $\mathcal{T}$ much longer than the natural time scale of the laser. The choice of $\mathcal{T}$ is based on the observation that, very roughly the

spectrum in Fig. 5 suggests that the corresponding intensity pattern is the superposition of weakly correlated modes each oscillating at slightly different frequencies. Therefore we can expect the recurrence time of the dynamics to be of the order of the longest beating period between modes. We choose the averaging time $\mathcal{T}$ to be much longer than this estimate of the recurrence time.

The requirement that the average intensity pattern is well approximated by a linear superposition of the intensities of the modes implies that

$$\langle f_j \bar{f}_k \rangle_{\mathcal{T}} = \delta_{jk} C_k, \qquad (6)$$

where δ_{jk} is Kronecker's δ function and the C_k is the average intensity of the mode k. However, we can expect situations in which the above equation is not valid. This is the case, for instance, when only two nearly degenerate modes are present: the high pump solution is then a frequency locked combination of the two modes. The frequency locking allows a nontrivial interplay of phase invariance and spatial symmetry that can lead to "tilted" average patterns with maxima on an axis tilted at $\pi/4$ with respect to the symmetry axes of the laser [14]. With more than two modes, this type of patterns can be observed when all modes of different parity with respect to inversion are frequency locked. With several active modes, this type of pattern is expected to be quite difficult to observe. More generally, there are two cases when $\langle f_j \bar{f}_k \rangle_{\mathcal{T}}$ is negligible. In the first, the Fourier spectra of the amplitudes do not overlap: more precisely

$$|g_j(\omega)\bar{g}_k(\omega')| \ll 1 \text{ if } |(\omega-\omega')| < 2\pi/\mathcal{T}, \qquad (7)$$

where $g_j(\omega)$ is the Fourier transform of $f_j(t)$. In the second case, condition (7) is not satisfied but there is a very strong phase noise. Nonlinear oscillations of the amplitudes of the modes produce also a broadening of their Fourier spectra. Therefore we expect that average amplitude products will increase in strength at higher pump energies.

From Eq. (5), one can see that the intensity of single mode solutions is even under inversion and under reflections with respect to the x and y axes. However, in general multimode solutions are composed by modes with different transformation properties. From Eq. (5) we know that in this case the average patterns are in general not symmetric. However, the symmetry of a pattern is not an "all or nothing" property: a pattern can be "nearly" symmetric in the sense that a small perturbation can make it symmetric. Moreover, the amount of symmetry breaking is related to the overlap of the mode spectra. It is therefore important to define a measure of the symmetry of a pattern that can be used not only to ascertain whether a pattern is or is not symmetric, but also how far away from symmetry it may be. As an example, if γ is a spatial transformation we can use as a measure of the symmetry with respect to γ of a pattern $G(\boldsymbol{x})$ the function $S(\gamma, G)$ defined as

$$S(\gamma, G) = \frac{\|G(\boldsymbol{x}) - G(\gamma\boldsymbol{x})\|_2^2}{\|G(\boldsymbol{x})\|_2^2} \equiv \frac{\int_{\mathbb{R}^2} |G(\boldsymbol{x}) - G(\gamma\boldsymbol{x})|^2 dxdy}{\int_{\mathbb{R}^2} |G(\boldsymbol{x})|^2 dxdy}.$$

$$(8)$$

If γ is a symmetry of the pattern $G(\boldsymbol{x})$ then $S(\gamma,G)=0$. Moreover, if γ is "nearly" a symmetry then we can expect $S(\gamma,G)$ to be small. In the rest of this section, when we write that a pattern $G(\boldsymbol{x})$ has symmetry γ we imply that $S(\gamma,G) < \varepsilon$, where $\varepsilon \ll 1$. What may be a reasonable choice of the value of ε is an open question, to which we return in the conclusions.

A very useful property of S is that it is possible to relate the breaking of a symmetry with respect to reflections σ_x and σ_y or inversions R_π (rotations by π with respect to the origin), to the magnitude of some of the products $\langle f_j \bar{f}_k \rangle_{\mathcal{T}}$. For example, if we indicate with $G(\boldsymbol{x})$ the average intensity pattern defined in Eq. (5), then, a pattern is symmetric with respect to reflections about the x axis if

$$S(\sigma_x, G) < \varepsilon \Leftrightarrow \frac{\|2 \sum \langle f_j \bar{f}_k \rangle_{\mathcal{T}} \bar{A}_k A_j\|_2^2}{\|G\|_2^2} < \epsilon,$$

where the sum is only over the modes with different parity with respect to σ_x. We can use this property to infer from the symmetry of the average intensity patterns specific bounds on the average amplitude products.

Considering the possible presence of non-vanishing amplitude products, but excluding the frequency locking described before, the following types of patterns may arise (see Fig. 4 for a pictorial representation of all these cases).

Type I: The average intensity pattern (5) is even (invariant) under reflections and inversion if and only if all the average products $\langle f_j \bar{f}_k \rangle_{\mathcal{T}}$ between modes with different transformation properties are small, i.e., if

$$S(\sigma_x, G) < \varepsilon, \ \ S(\sigma_y, G) < \varepsilon, \ \ S(R_\pi, G) < \varepsilon.$$

Nonzero average amplitude products between modes with the same transformation properties does not break any invariance and can be added to each of the following cases without altering the result.

Type II: The average pattern is invariant under inversion, but not under reflection,

$$S(\sigma_x, G) > \varepsilon, \ \ S(\sigma_y, G) > \varepsilon, \ \ S(R_\pi, G) < \varepsilon,$$

if the only average amplitude product between modes with different transformation properties that is small is between modes of the same parity with respect to inversion (modes with m of the same parity) and of different parity with respect to reflections.

Type III: The average intensity is invariant with respect to one axis, but not with respect to inversion,

$$\left. \begin{array}{ll} \text{either} \ \ S(\sigma_x, G) < \varepsilon, & S(\sigma_y, G) > \varepsilon, \\ \text{or} \ \ S(\sigma_y, G) < \varepsilon, & S(\sigma_x, G) > \varepsilon, \end{array} \right\} \text{ and } S(R_\pi, G) > \varepsilon,$$

if the only average amplitude product between modes with different transformation properties that is small is between modes of the same parity with respect to either σ_x or σ_y, but of different parity with respect to inversion (modes with m of different parity). The symmetry axis is x or y if the modes have the same transformation properties with respect to σ_x or with respect to σ_y.

Type IV: The average pattern does not have any symmetry,

$$S(\sigma_x, G) > \varepsilon, \ \ S(\sigma_y, G) > \varepsilon, \ \ S(R_\pi, G) > \varepsilon.$$

if average amplitude products as in types II and III are significantly different from zero or there are at least two pairs of non vanishing amplitude products as in type III preserving the invariance with respect to different axes.

In general, the observation of the evolution of an average pattern from the "most symmetric" case (type I) to one of the other "less symmetric" cases cannot be considered in a strict mathematical sense an example of symmetry breaking, as the symmetry of type I patterns is in general not exact. However, the observation of a transition between different types of patterns enables us to assess the presence of nonvanishing amplitude products between modes of different parity directly from the average patterns. This is a very simple way to have experimental indication on the frequency spectra of the mode dynamics in very fast systems. As an example of the type of information provided by this analysis, the observation in astigmatic lasers of average patterns not invariant with respect to both symmetry axes provides a clear indication that the assumption that multimode laser emission is due to the incoherent superposition of modes is in many cases wrong: the absence of symmetry is a clear indication that modes of different parities are correlated one to the other.
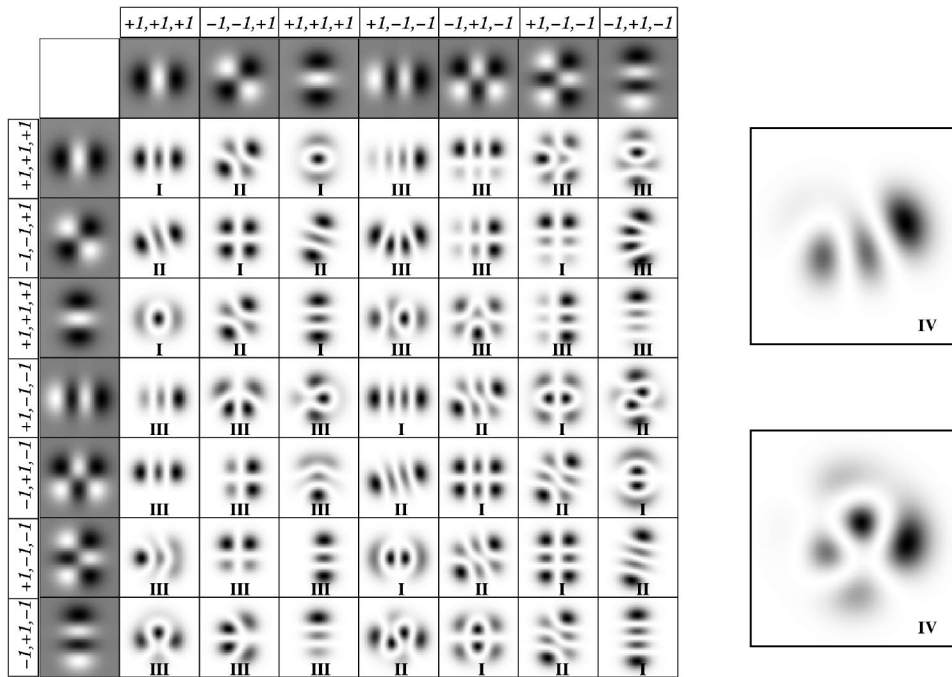
FIG. 4. Examples of intensity patterns of sums of modes with various types of symmetry. The images in the grey lines are the Gauss-Hermite modes with indices $p=\{2,1,0,3,2,1,0\}$ and $q=\{0,1,2,0,1,2,3\}$ (families with $m \equiv p+q = \{2,3\}$, respectively) from left to right and top to bottom. The numbers above or to the left of each mode represent their parity with respect to σ_x, σ_y, and R_π (rotations by π), respectively. The pattern at the crossing of row j and column k is a grey scale image of the intensity of mode k plus one half of mode j. The letters on each intensity pattern refer to the classification given in the text. The two patterns of type IV on the right-hand side are the sum of the modes (2,0), (1,1), and (3,0) (top: case of type II and type III product both significantly different from zero) and (2,0), (3,0), and (0,3) (bottom: case of two type III products both significantly different from zero, but with respect to different axes).

Note that for the last two types of patterns there must be at least two families with different transformation properties under inversion. For modes almost unaffected by the aperture, this implies that near and far field are different because the difference of the Gouy phase for modes with m of different parity is an odd multiple of π [22]. Furthermore, a pattern in region 4 of Fig. 1, without any symmetry, but with the far field that is just a rescaled version of the near field shows unambiguously that the the cavity does not possess any symmetry. Therefore, the study of these patterns can provide a simple way to assess experimentally the presence of misalignments in a supposedly astigmatic cavity. It is straightforward to adapt this analysis to a different way of measuring the symmetry breaking, such, for instance, one based on the maximum of $G(\mathbf{x}) - G(\gamma\mathbf{x})$.

V. SYMMETRY ANALYSIS OF AVERAGE INTENSITY PATTERNS

In order to validate the model described by Eqs. (1)–(3) we have run a set of simulations to verify whether it could reproduce the experimentally observed average patterns. To this purpose we have written two integration routines. The first integrates the integro-differential equations (1)–(3) by representing the three fields F, P, and N on a rectangular grid with periodic boundary conditions. The cavity propagation operator P, Eq. (A5), has been rewritten in terms of convolution products that can be efficiently computed using fast

Fourier transforms. The ordinary differential equations that represent the evolutions of F, P, and N on the grid points are integrated using the variable-step–variable-order routine ODE of the NETLIB library [25]. This code makes no assumptions on the dynamics of the laser, but is rather slow. We have therefore used it only to check that the results of the second code are reliable.

The second code is composed of two parts: the first finds the modes of the cavity, the second integrates the equations for the modal amplitudes. We have used the routine ZGEEV of the Lapack library [26] to find the cavity modes by computing the representation of the right and left modes of P, $A_k(\mathbf{x})$, and $B_k(\mathbf{x})$, respectively, on the basis of the Gauss-Hermite modes.

Once the modes of the cavity are known, it is possible to project Eq. (1) onto them and obtain a set of ordinary differential equations for the amplitudes of the modes

$$\frac{d}{dt}f_k = \mu_k f_k + (B_k, P)_X. \tag{9}$$

We have used a Gaussian quadrature algorithm to compute the projection integral in Eq. (9) and have represented the fields P and N on the nodes of the quadrature. The ordinary differential equations for the amplitudes of the modes and for the values of the fields P and N on the nodes have been integrated using the routine ODE. This program is much faster than the first one because fewer points are needed to
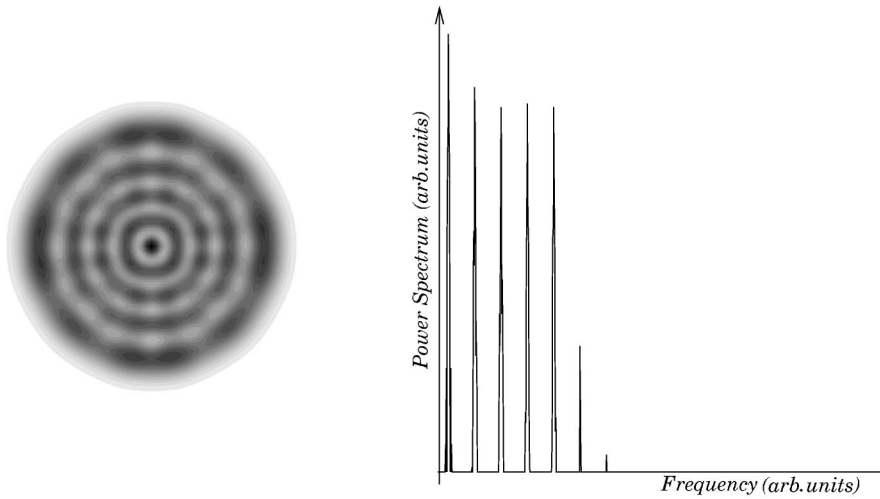
FIG. 5. Gray scale image (black high intensity) of the average intensity pattern of a 0-0 pattern (left) and power spectrum of the intensity measured at the center of the image. Cavity parameters as in the top center of Fig. 6. Simulation parameters $\gamma=0.025$, $R=0.94$, $\delta_A=-2.76$, $\chi=1.3$, super-Gaussian pump of width 7.0, 48×48 grid points, integration time was 60 000 time units. The average intensity was computed using only the last 30 000 time units of the simulation data.

compute accurately the projection integral in Eq. (9) than the propagation operator in Eq. (1). Moreover, the number of relevant modes can be very small, as only the active modes need to be considered.

We have analyzed numerical simulations from five to roughly fifty active modes for a ring laser where the propagation from the aperture to the active medium is represented by the same *ABCD* matrices of the Fabry-Pérot cavities used in Refs. [1,3]. As our working hypothesis is that the average intensity patterns are independent of the nature of the active medium, we have chosen the medium parameters in the simulations to be relevant to the experiments of Refs. [1,3], but with no claim to give a faithful representation of the active medium used in the experiment. Therefore, in all

simulations we have set the decay rate of the population inversion to $0.1\geqslant\gamma\geqslant0.001$ in units of the polarisation decay time, the cavity round-trip time to $T_c=1$ in the same units and the mirror reflectivity to $R=94\%$.

We have run hundreds of simulations and have recorded the average intensity patterns of each of them. As in the experiments, we concentrate initially on regular patterns. We have reproduced the patterns of type 1-1, 1-0, and 0-0 of Refs. [1,3] (see Fig. 5 for a 0-0 pattern and the top left and center images in Fig. 6 for a 1-1 and 1-0 pattern, respectively) in some range of parameters.

These patterns have two orthogonal symmetry axes and, in terms of symmetry and average amplitude products, are part of the larger family of patterns of type I, according to
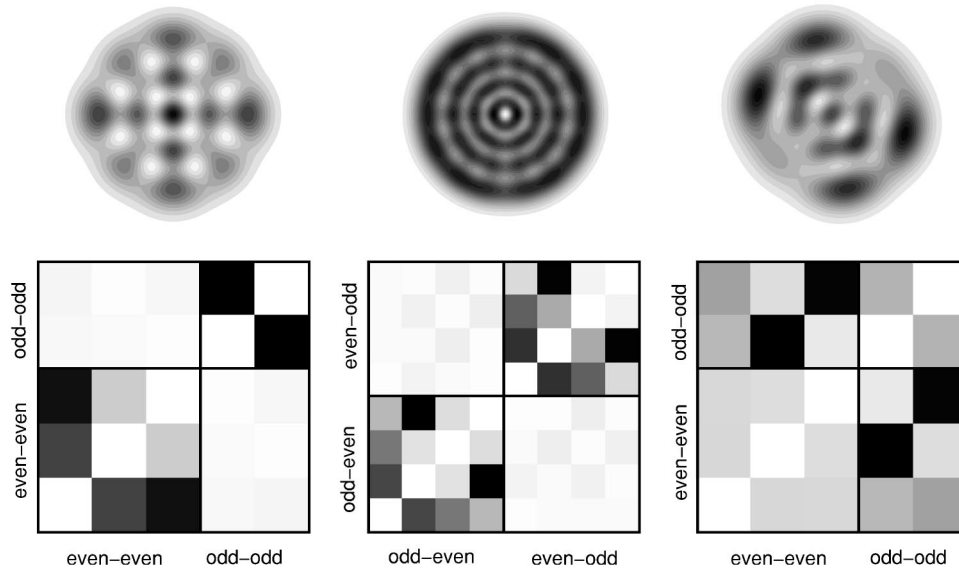
FIG. 6. Average patterns and their average amplitude products. Gray scale images (black high intensity) of average intensity patterns (top) and of the corresponding average amplitude products between modes (bottom). The names of the groupings, e.g., "even-odd," refer to the symmetry of the modes with respect to σ_x and σ_y. See text for more details. The highest values of the product are $\{0.30, 0.06, 0.93\}$. Cavity parameters. Left and right images: $A_x=D_x=0.931\,5554$, $B_x=0.037\,6978$, $A_y=D_y=0.929\,3088$, $B_y=0.038\,889\,879$, on axis circular aperture with radius $R_A=3.0$. Center image: $A_x=D_x=0.924\,696$, $B_x=0.025\,300$, $A_y=D_y=0.921\,026$, $B_y=0.026\,482\,76$, on axis circular aperture with radius $R_A=3.5$. In both cases 256×256 grid and 496 Gauss-Hermite modes were used to obtain the cavity modes. Simulation parameters $R=0.94$, $\delta_A=\{1.876, 3.12, 1.876\}$, pump either flat (left and center) or Gaussian of width 3.25 (right) with amplitude $\chi=\{1.55, 1.15, 2.8\}$, 48×48 grid points, integration time was 80 000 time units. The average intensity and the products were computed using only the last 40 000 time units of the simulation data.

the classification in Sec. IV. More specifically, they are made up by modes of a single family which are only weakly perturbed by the aperture: each mode is composed by a strongly dominant Gauss-Hermite mode with a small contribution from the other Gauss-Hermite modes. As a rule of thumb, two conditions for the numerical observation of these patterns are that the fraction of gain line above threshold is not larger than the frequency separation $\Delta\nu_T$ between consecutive families of modes and that the index of the resonant family is $m < m_M$. The energy distribution among the modes of these patterns is in agreement with what is described in the experimental section. The structural changes of average patterns for fixed detuning and increasing pump are as follows. If the laser is resonant with a family of index m, then, increasing the pump, the laser goes from a single mode solution, with a very small region of stability, to a "target pattern" with almost cylindrical rings in which all modes of the resonant family have similar energy. In between these two regimes, one can observe tilted average patterns due to mode locking, but their window of stability is quite small. Further increasing the pump, one can observe a regular pattern of type 0-0 or 1-1 if m is even and regular patterns of type 1-0 or 0-1 if m is odd. For target patterns and regular patterns, nonvanishing average amplitude products are observed only between modes with the same transformation properties. The regular structure is lost at higher values of the pump, either through a change in the distribution of energy among the family modes, or through the appearance of modes of a different index. Due to the broadening of the modes' spectra at higher pump, it is often possible to observe nonvanishing products that lead to breaking of the average symmetry. Starting instead from a regular pattern made up by modes of the family with index m and changing detuning with fixed pump, we observe loss of regularity due to some modes going off resonance and others getting into resonance. These results allow us to provide a qualitative explanation of the features of Fig. 1. No regular patterns can be observed for detuning $\Delta\nu_T \sim \Delta\nu_a$, as in this case families of different index m are not separated in frequency from one another. Incidentally, we note that this is the region where it is most likely to observe patterns of types III and IV with average amplitude products between modes with different indexes m. Beyond this very narrow region (not shown in Fig. 1), there is a boundary between the zone where regular patterns are observed and the zone where they are not observed. The presence of this boundary and its quadratic dependence on $\Delta\nu_T$ can be explained as follows. As N_f increases, the number of families with very similar losses increases. It is then necessary to have larger values of $\Delta\nu_T$ to be able to have only one active family. The quadratic dependence of the boundary from $\Delta\nu_T$ is due to the quadratic dependence of the gain from $\Delta\nu_T$. The observation for the same value of the pump of a different regular pattern made up by modes of the family with index $m' \neq m$ is possible if the losses of the modes of the two families are similar and if $m' < m_M$. Due to the dependence of losses from the aperture, the likelihood of this event increases with N_f.

The comparison between regular patterns in numerical simulations of Eqs. (1)–(3) and in the experimental results of Refs. [1,3] shows that the model proposed in this paper is certainly a valid tool for the analysis of average intensity patterns in lasers. In particular, the model described by Eqs. (1)–(3) is ideally suited to analyse in detail the connection between symmetry and average amplitude products predicted in the previous section because of its faithfulness to the experiment and its computational efficiency.

A first result is shown in Fig. 6 where the average amplitude product between modes are shown underneath the corresponding average intensity patterns. The shading of the square in row i and column j in the product checker-boards corresponds to the average product between the cavity modes i and j, with black (white) indicating highest (zero) average product. In all three cases the modes all belong to a single family with number of modes $m=\{4,7,4\}$ from left to right. The average intensity of each mode has been artificially set to zero. The modes have been grouped according to their parity with respect to σ_x and σ_y. In the case of the patterns on the left and at the center of Fig. 6, symmetric with respect to σ_x and σ_y, the average amplitude products between modes of the same parity are much stronger than between modes of different parity. In the case of the rightmost pattern the products between modes of opposite parity are particularly strong and the only symmetry of the average pattern is the inversion with respect to the origin.

The simulations confirm the importance of including astigmatism and symmetry breaking in the model. Average patterns in an astigmatic laser (top left of Fig. 6) differ substantially from average patterns in a laser with cylindrical symmetry (Fig. 7) even for values of the pump for which the solutions are no longer symmetric. This is due to the fact that the spatial structure of the cavity modes and their losses or gains are affected by the overall symmetry of the system, even when the symmetry in the spatio-temporal solutions is fully broken.

VI. CONCLUSION

Average intensity patterns are fundamental to the study of multimode dynamics in intermediate Fresnel number lasers because they are essentially the only patterns that can be studied experimentally. The temporal behaviour of the intensity can be measured only at a few points in the transverse section of the beam. It is even harder to measure the phase of the field.

In this paper we have highlighted some of the intriguing features of these patterns and have shown what information can and cannot be gleamed from them. The laser dynamics in the parameter regions studied here is often irregular. Moreover, simulations with the same parameter values but different initial conditions may evolve in different regions of phase space (even though it is not possible to exclude that the full exploration of the available phase space takes a time much longer than the ones we used in the numerical integrations).

Yet, we have shown that when specific conditions on the dynamics and the average time are satisfied, average intensity patterns are almost stationary and do not depend much on the details of the dynamics or to the parameters of the lasers. In other words, there are conditions under which av-
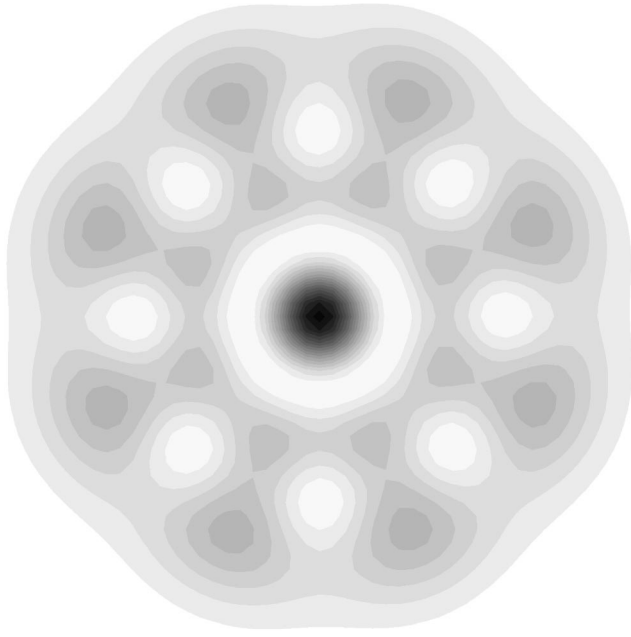
FIG. 7. Gray scale image (black high intensity) of the average intensity pattern of an axially symmetric laser. This figure should be compared with the pattern on the left of Fig. 6 obtained for an astigmatic cavity. The parameters are the same as in the left pattern of with the exception that the cavity parameters in the x and y directions are the same.

erage patterns have universal features. This is confirmed experimentally by the fact that the same type of patterns have been observed in very different types of lasers. Indeed we have shown in Sec. V that the amount of symmetry breaking of average patterns of an astigmatic laser, assuming perfect D_2 symmetry, is a good indication of the overlapping of frequency spectra between different families of modes. For example, even though the dynamics may be irregular, from the average symmetry we can infer features of the spectra of the cavity modes.

The importance of the symmetry of the pattern begs the question of how this can be measured and how sensitive the measure is to experimental artifacts. In this paper we have introduced the function $S(\gamma,G)$ defined in Eq. (8), to measure the symmetry of a pattern $G(x)$ with respect to a symmetry γ. However, the interpretation of its values (and, hence, the choice of the parameter ε in the analysis in Sec. IV) is not straightforward and requires a precise knowledge of the cavity modes. Consider the numerical pattern shown at the top center of Fig. 6. This pattern appears to have reflection symmetry with respect to the horizontal and the vertical. We have therefore computed $S(\gamma,G)$ for this pattern where $\gamma \equiv \gamma(\theta)$ is the reflection with respect to an axis that forms an angle θ with the horizontal. Its graph as a function of θ is shown on the left-hand side of Fig. 8. The function is zero at $\theta=\{0,\pi/2\}$ as expected. However, its value is always very small, a consequence of the fact that the modulation of the intensity on the rings is very small: in other words, according to this measure the pattern has "nearly" cylindrical symmetry because the depth of the modulation of the rings is relatively small. As another example, consider the leftmost image in
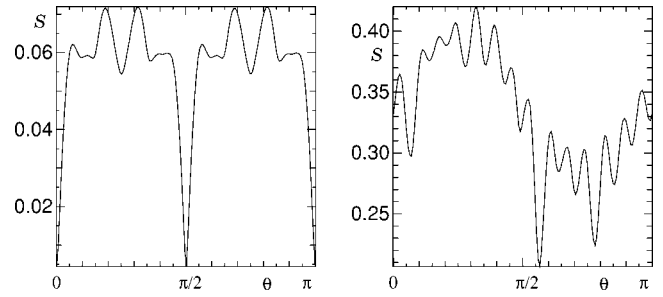
FIG. 8. Plots of $S(\gamma,G)$, where γ is the reflection with respect to an axis at an angle θ with the horizontal. The pattern G used for the left graph is the average intensity pattern shown in the top center of Fig. 6. The one used for the right graph is the experimental pattern furthest to the left in Fig. 2

Fig. 2: we can see that the illumination of the beam is not uniform, probably due to some residual misalignment that is small enough not to affect the geometry of the pattern. The image looks similar to having two axes of symmetry slightly tilted with respect to the horizontal and the vertical. This impression is confirmed by the graph of S shown on the right-hand side of Fig. 8, but it is an open question how significant a measure of symmetry the troughs and peaks of this graph are when compared to the average value of S. Moreover, the minimum at $\theta \simeq 3/4\pi$ is much smaller than the minimum at $\theta \simeq \pi/20$ even though the latter corresponds to a "real" symmetry of the pattern while the former is an artifact of the nonuniform illumination. Definite answers to these problems can only be obtained by new experiments targeted at measuring the intrinsic symmetries of the patterns and by further refining theoretical tools to measure symmetry, of which Eq. (8) is just a first example.

APPENDIX: DERIVATION OF THE MODEL

For simplicity we assume that the laser under study is a ring cavity gas laser with approximate cylindrical symmetry. In deriving the model we follow Refs. [24,27]. We represent the electric field $\hat{F}$ with a scalar slowly varying amplitude [28] F,

$$\hat{F}(x,y,z,t) = \frac{1}{2}[F(x,y,z,t)e^{i(k_A z - \omega_A t)} + \text{c.c.}]. \quad (A1)$$

We adopt a Maxwell-Bloch model for the active medium, described a polarization $\hat{P}$ and a population inversion N. Moreover, the amplitude $\tilde{P}$ of the polarization is also slowly varying:

$$\hat{P}(x,y,z,t) = \frac{1}{2}\left[\tilde{P}(x,y,z,t)e^{i(k_A z - \omega_A t)} + \text{c.c.}\right]. \quad (A2)$$

In Eqs. (A1), (A2) $\omega_A = c k_A$ is the frequency of the atomic transition, with c the speed of light and k_A the corresponding wave number. All the coordinates in these equations are nondimensional: the longitudinal coordinate z that runs along the axis of the cavity is scaled with the cavity length L_C so that the dependence of any field on z is periodic of period 1. Time

t is scaled to the polarisation decay time. The transverse coordinates x and y are scaled to the minimum beam waist in their respective directions w_x and w_y. The amplitudes F and P are assumed to be varying in z and t much more slowly than k_A and ω_A (slowly varying approximation) so that the second derivatives of F and $\tilde{P}$ with respect to z and t in Maxwell's wave equation can be neglected with respect to their first derivatives [28].

We set the origin of the z coordinate at the entrance of the active medium. This therefore occupies the region $0 \leqslant z \leqslant L$. The aperture is located at the exit of the active medium ($z = L$) and is assumed to be infinitely thin, perfectly absorbing and with negligible edge effects. It is represented in this model as a Θ function

$$\Theta_A(x,y) = \begin{cases} 1 & \text{if } (x,y) \text{ is inside the aperture,} \\ 0 & \text{otherwise.} \end{cases} \tag{A3}$$

Finally, for convenience sake we assume that the plane of the aperture is a symmetry plane of the cavity. This assumption is not essential for the validity of the following steps, but makes the algebra a little simpler. The derivation of the model consists of four parts.

(i) *Propagation outside the active medium.* The propagation of the slowly varying amplitude of the electric field in the part of the cavity outside the active medium is represented by a propagation operator $\mathcal{P}$ that relates the field at the entrance of the active medium to that immediately after the aperture

$$F(x,y,1,t) = \mathcal{P}\Theta_A F\left[x,y,L,t - \frac{1-L}{c}\right]. \tag{A4}$$

In terms of the *ABCD* matrices [18] of the cavity in the (x,z) plane (A_x, B_x, C_x, D_x) and the (y,z) plane (A_y, B_y, C_y, D_y), the propagation equation (A4) can be written as

$$F(x,y,1,t)$$
$$= \frac{-\operatorname{Re}^{i\delta_A}}{\pi\sqrt{B_x B_y}} \int_A e^{-(i/B_x)(A_x\xi^2 - 2x\xi + D_x x^2) - (i/B_y)(A_y\eta^2 - 2x\eta + D_y y^2)}$$
$$\times F\left[\xi,\eta,L,t - \frac{1-L}{c}\right] d\xi\, d\eta, \tag{A5}$$

where $\delta_A = k_A \bmod_{2\pi}$ is the phase shift accumulated by the reference frequency per round trip. We have included the effect of the aperture by restricting the integration domain to its area, as indicated by the symbol $\int_A$. The coefficient R is the total reflectance of the mirrors in the cavity and measures the amplitude loss during propagation. This equation or, equivalently, Eq. (A4) express the boundary conditions for the evolution of the field inside the active medium.

(ii) *Propagation in the active medium.* The equation for the propagation of the electric field in the active medium is most conveniently written in terms of the variables [24]

$$t' = t + \frac{1-L}{L}\frac{z}{c}, \quad z' = z \tag{A6}$$

and reads

$$\frac{\partial F}{\partial z'} + \frac{1}{cL}\frac{\partial F}{\partial t'} = \alpha\tilde{P} + \mathcal{Q}_M F, \quad 0 \leqslant z' \leqslant L. \tag{A7}$$

The coefficient α is a coupling constant between the electric field and the medium and ultimately represents the gain seen by the field. The linear operator $\mathcal{Q}_M$ represents the effect of the propagation inside the medium. We assume that it is independent of the longitudinal coordinate z, i.e., we assume that the active medium is optically homogeneous in the longitudinal direction.

In the coordinates (A6) the boundary condition (A4) on Eq. (A7) becomes an equal time boundary condition

$$F(x,y,0,t') = P\Theta_A F(x,y,L,t'). \tag{A8}$$

(iii) *The mean field limit.* The only essential hypothesis underlying Eq. (A7) and its boundary condition is the slowly varying amplitude approximation. In order to simplify them further we introduce the fields F' and $\tilde{P}'$ defined as averages of F and $\tilde{P}$, respectively, over $z\prime$ at $t\prime$ fixed:

$$F'(x,y,t') \equiv \frac{1}{L}\int_0^L F(x,y,z',t')dz',$$

$$\tilde{P}'(x,y,t') \equiv \frac{1}{L}\int_0^L \tilde{P}(x,y,z',t')dz'. \tag{A9}$$

Note that this average corresponds to an average over z (unprimed coordinate) along the active medium and an average over t over one cavity round trip. We ultimately want to use these average fields to represent the exact fields F and P. For this to be a valid approximation, we must therefore assume that the space-time variations of F (and, eventually, P) are on a length scale longer than the length of the active medium and on a time scale longer than the cavity round trip (i.e., low gain and mirror reflectivity close to 1). This approximation holds in the CO_2 laser described in Sec. II where the ratio of the saturated gain to the loss coefficients is of the order of 10.

We average Eq. (A7) according to Eqs. (A9) use (A8) and take the limit of infinitely short active medium ($L \rightarrow 0$) to obtain

$$\frac{\partial F'}{\partial t'} = -c[\operatorname{Id} - \mathcal{P}\Theta_A]F'(x,y,L,t') + \chi\tilde{P}', \tag{A10}$$

where $\mathcal{P}$ is the propagator across the entire cavity starting at $z = 0$ and $\chi \equiv \alpha L$, is the gain per unit pass (pump parameter).

(iv) *The material equations.* Equation (A10) for the electric field must be coupled to the equations for the polarization and the population inversion. For a standard Maxwell-Bloch model of a two-level system these can be written as

$$\frac{\partial\tilde{P}}{\partial t} = -\tilde{P} + F + \tilde{N}F, \tag{A11}$$

$$\frac{\partial \widetilde{N}}{\partial t} = -\gamma \left[\widetilde{N} + \frac{1}{2}(\bar{F}\widetilde{P} + \text{c.c.}) \right], \qquad (A12)$$

where γ is the population inversion decay rate. We apply to these equations exactly the same procedure followed for the electric field. In particular, we change variables according to Eq. (A6) and average as in Eq. (A9). In doing so we assume that the material is homogeneous along the cavity axis and that the variations of the two fields with z are sufficiently small that we can approximate the average of the product with the product of the averages. As a final step, we scale the polarization and the population inversion with the pump parameter $P' = \chi \widetilde{P}$ and $N' = \chi \widetilde{N}$, so that Eq. (A10)–(A12) become

$$\frac{\partial F}{\partial t} = \mathcal{L}F + P, \qquad (A13)$$

$$\frac{\partial P}{\partial t} = -P + \chi F + FN, \qquad (A14)$$

$$\frac{\partial N}{\partial t} = -\gamma \left[N + \frac{1}{2}(F\bar{P} + \bar{F}P) \right], \qquad (A15)$$

where we have dropped all the primes and where $\mathcal{L} \equiv -c[\text{Id} - \mathcal{P}\Theta_A]$. These equations constitute the model that we analyze in this paper.

Before concluding this section we remark that it is possible to derive equations similar to Eqs. (A13)–(A15) for a Fabry-Pérot cavity provided that the population inversion grating induced by the standing wave nature of the electric field can be neglected [29]. The main obstacle in the derivation is the expression of the boundary conditions in terms of the propagation operator.

---

[1] D. Dangoisse, D. Hennequin, C. Lepers, E. Louvergneaux, and P. Glorieux, Phys. Rev. A **46**, 5955 (1992).

[2] G. Huyet, M. C. Martinoni, J. R. Tredicce, and S. Rica, Phys. Rev. Lett. **75**, 4027 (1995).

[3] E. Louvergneaux, D. Hennequin, D. Dangoisse, and P. Glorieux, Phys. Rev. A **53**, 4435 (1996).

[4] Y. F. Chen and Y. P. Lan, Phys. Rev. A **65**, 013802 (2002).

[5] J. Farjas, D. Hennequin, D. Dangoisse, and P. Glorieux, Phys. Rev. A **57**, 580 (1998).

[6] L. Ning, Y. Hu, R. E. Ecke, and G. Ahlers, Phys. Rev. Lett. **71**, 2216 (1993).

[7] B. J. Gluckman, P. Marcq, J. Bridger, and J. P. Gollub, Phys. Rev. Lett. **71**, 2034 (1993).

[8] E. Bosch, H. Lambermont, and W. van de Water, Phys. Rev. E **49**, 3580 (1994).

[9] B. J. Gluckman, C. B. Arnold, and J. P. Gollub, Phys. Rev. E **51**, 1128 (1995).

[10] S. Rudroff and I. Rehberg, Phys. Rev. E **55**, 2742 (1997).

[11] V. M. Eguíluz, P. Alstrøm, E. Hernández-García, and O. Piro, Phys. Rev. E **59**, 2822 (1999).

[12] F. Encinas-Sanz, I. Leyva, and J. M. Guerra, Phys. Rev. A **62**, 043821(11) (2000).

[13] F. Encinas-Sanz, O. G. Calderón, R. Gutiérrez-Castrejón, and J. M. Guerra, Phys. Rev. A **59**, 4764 (1999).

[14] D. R. J. Chillingworth, G. D'Alessandro, and F. Papoff, Physica D **177**, 175 (2003).

[15] J. Lega, J. V. Moloney, and A. C. Newell, Phys. Rev. Lett. **73**, 2978 (1994).

[16] J. Lega, J. V. Moloney, and A. C. Newell, Photochem. Photobiol. **83**, 478 (1995).

[17] G. D'Alessandro and F. Papoff (unpublished).

[18] A. E. Siegman, *Lasers* (University Science, Mill Valley, California, USA, 1986).

[19] M. Brambilla, F. Battipede, L. A. Lugiato, V. Penna, F. Prati, C. Tamm, and C. O. Weiss, Phys. Rev. A **43**, 5090 (1991).

[20] C. Green, G. B. Mindlin, E. J. D'Angelo, H. G. Solari, and J. R. Tredicce, Phys. Rev. Lett. **65**, 3124 (1990).

[21] D. Hennequin, C. Lepers, E. Louvergneaux, D. Dangoisse, and P. Glorieux, Opt. Commun. **93**, 318 (1992).

[22] E. Louvergneaux, G. Slekys, D. Dangoisse, and P. Glorieux, Phys. Rev. A **57**, 4899 (1998).

[23] E. A. Sziklas and A. E. Siegman, Appl. Opt. **13**, 2775 (1974).

[24] L. A. Lugiato, G.-L. Oppo, J. R. Tredicce, L. M. Narducci, and M. A. Pernigo, J. Opt. Soc. Am. B **7**, 1019 (1990).

[25] Routine ODE from the package ODE of NETLIB, URL http://www.netlib.org

[26] Library LAPACK at NETLIB, URL http://www.netlib.org/lapack/

[27] A. G. Fox and T. Li, Bell Syst. Tech. J. **40**, 453 (1961).

[28] O. Svelto, *Principles of Lasers* 4th ed. (Plenum, New York, 1998).

[29] F. Papoff and G. D'Alessandro, J. Opt. Soc. Am. B **2**, 367 (2000).